International Forum on Aeroelasticity and Structural Dynamics
IFASD 2017
25-28 June 2017 Como, Italy

CLOSED-LOOP FLIGHT TESTS WITH AN UNMANNED EXPERIMENTAL MULTI-BODY AIRCRAFT

Alexander Köthe[1], Alexander Behrens[1], Alexander Hamann[1], Phillip Nagel[1], Danny Nowka[1], Robert Luckner[1]

[1]Technische Universität Berlin - Institut für Luft- und Raumfahrt
Marchstraße 12,10587 Berlin, Germany
alexander.koethe@campus.tu-berlin.de, alexander.behrens@ilr.tu-berlin.de,
alexander.hamann@tu-berlin.de, phillip.nagel@campus.tu-berlin.de,
danny.nowka@campus.tu-berlin.de, robert.luckner@tu-berlin.de

Keywords: Wind Tunnel and Flight Testing, Highly Flexible Aircraft Structures, Active Control and Adaptive Structures

Abstract: At TU Berlin's department of Flight Mechanic, Flight Control and Aeroelasticity the concept of a Multi-Body High Altitude Pseudo Satellite aircraft is investigated for surveillance and communication tasks. This aircraft consists of several individual aircraft that are coupled in the mission altitude to a formation with a high aspect ratio. The aircraft was designed for a continuous one year mission in 20 km height based on the DARPA Vulture program specification. Based on a suitable flight dynamic model, the flight control laws for flight path control were designed and verified in closed-loop nonlinear simulation studies. A validation of the new control law approach for a Multi-Body aircraft is missing. In this paper, a small scaled Experimental Multi-Body aircraft is used to validate the control laws in flight test. Besides the flight dynamics and flight control law design, the paper describes the experimental setup in detail.

1 INTRODUCTION

High Altitude Pseudo Satellites (HAPS) aircraft have become an interesting alternative for satellites, e.g. for communication and surveillance tasks, since they offer more flexibility in operation. Due to their lightweight construction, their high-aspect-ratio and the use of solar panels, they can be operated in the stratosphere for up to 336 hours (cf. QinetiQ Zephyr [1]). In contrast to satellites, HAPS aircraft are not bound to a specific trajectory. They can be operated in a specific region for a certain amount of time. When a mission is completed, they can be recovered, relocated and used for another mission. Current HAPS aircraft have large wing spans that can lead to large deformation caused by aerodynamic loads. Especially if a HAPS aircraft passes the troposphere, high aerodynamic loads can occur. Additionally, the aeroelastic and flight dynamic modes can couple with each other since the high flexibility shifts the structural modes to lower frequencies. Those previously introduced physical problems of current HAPS led to mishaps with the NASA Helios, Google Solara [2] and Facebook Aquila [3]. Since the use of HAPS promises huge benefits, the question of a real alternative aircraft technology for the replacement of satellites still remains. A new alternative to single-wing HAPS aircraft are Multi-Body Aircraft (MBA) that are investigated at TU Berlin's department of Flight Mechanics, Flight Control and Aeroelasticity. This concept is based on the linkage of several individual rigid-body aircraft to a single HAPS aircraft in the mission altitude. A high-aspect-ratio can

Table 1: Properties of the Designed Multi-Body High Altitude Long Endurance Aircraft

Coupled aircraft	i	=	10		Mission altitude	H	=	20	km
Mission latitude	Lat	$\leq$	40°		Complete span width	b	=	215.27	m
Aspect ratio	Λ	=	66.76		Total mass	m	=	4089.9	kg
Design speed	V	=	33.15	$\frac{\text{m}}{\text{s}}$	Required energy	E_{req}	=	3.2212	GJ
Design lift coefficient	C_L	=	1.242		Zero drag coefficient	$C_{D,0}$	=	0.0061	
Total payload	m_{Pay}	=	450	kg	Required payload power	$P_{\text{req,pay}}$	=	5	kW

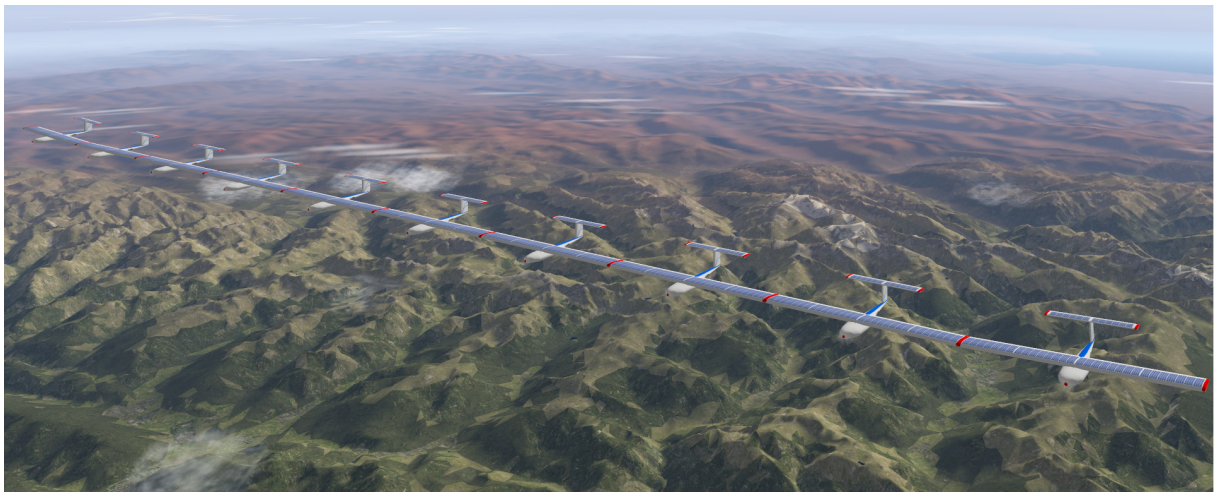

Figure 1: Illustration of the Designed Multi-Body High Altitude Long Endurance Aircraft

be accomplished without consideration of structural geometrical nonlinearities. Moreover, each single aircraft can be brought to the stratosphere with a helium balloon or fly on their own up to the mission altitude ensuring low aerodynamic loads and hence low bending moments caused by atmospheric disturbance in the troposphere. Lastly, the modularity of a MBA permits exchange and return to ground of a single individual aircraft for repairing purposes without significantly affecting the flight mission.

In the research project, a HAPS design was achieved that is capable to fulfill the DARPA Vulture program specifications completely [4]. A coupled formation of ten aircraft with a total aspect ratio of 66.76 is used as aircraft design. Details are listed in Table 1. In the design phase, the connection between the single aircraft was assumed to be rigid. In the flight dynamic investigation, the full equations of motion for the MBA were assembled with Kane method. A mechanical joint that allows roll and pitch motion between the aircraft was used as connection. The resulting flight dynamic model was nominal unstable. Figure 1 shows the final design including tail sizing. Stabilizing of the plant as well as automatic flight path control and low energy consumption was established with a flight control law that was designed in the frequency domain. Since one of the main objectives in the HELIOS investigation report was the consideration of nonlinear effects, nonlinear flight dynamics were modeled as uncertainties. The resulting flight control law was verified in nonlinear closed-loop simulations.

The idea of using coupled aircraft was already shown in practical application. Dr. Richard Vogt, a German engineer who immigrated to the United States considered such an idea already decades ago [5]. He proposed that extra floating panels carrying fuel tanks could be attached to wing tips with hinges to extend the effective wingspan of a larger aircraft. The effect would be a higher aspect ratio similar to a glider and, hence, an increase of the range. In 1949, a preliminary

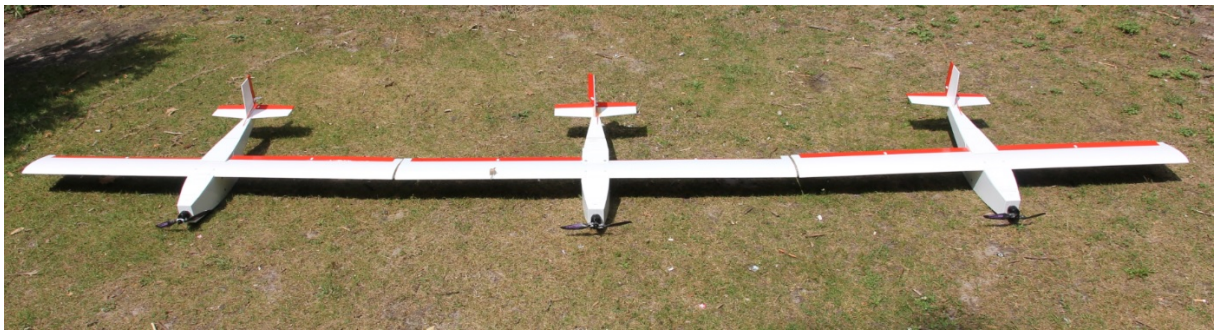

Figure 2: Experimental Multi-Body Aircraft

investigation was carried out in United States, in which a Culver Q-14 was successfully coupled to a Douglas C-47 and in total 230 tests were performed. After that test, the Tip Tow program started with the coupling of two Republic EF-84D Thunderjets to a Boeing EB-29A. The tests were successful and the technology of coupling aircraft was proven in real flight test. However, back then, every time pilots were in the flight control loop. A Multi-Body aircraft operating as HAPS is unmanned and, hence, the validation of the flight control laws in practical application is missing. For that reason, the theoretically verified flight control law structure for a Multi-Body aircraft shall be demonstrated in a flight test campaign.

In the flight test campaign, a small scaled Multi-Body aircraft with three coupled aircraft is used. The mechanical connection is similar to the one of the real HAPS application. Figure 2 shows the aircraft on the ground. The aircraft is remotely controlled by a pilot and hence only the inner-loops are tested in the flight tests. The total mass of the formation is 4.622 kg. The center aircraft is a little bit heavier than the two outer aircraft. The aircraft total span is 4.2 m (each aircraft has a span of 1.4 m) and an aspect ratio of 28 is established. In this paper, the flight dynamic model of the demonstrator aircraft is introduced. Afterwards, the flight control law design that is similar to the one for the real HAPS aircraft is described. Previous to the flight test results, the experimental setup including sensors and data communication between the aircraft is explained in detail. The main scope of this paper is the validation of the flight control laws for a Multi-Body aircraft in flight.

2 FLIGHT DYNAMICS OF MULTI-BODY AIRCRAFT

The equations of motion for the experimental Multi-Body aircraft are assembled following Kane's formalism [6] by using the software tool Autolev / Motion Genesis [7]. The methods are presented in detailed in two previous papers [8, 9]. Aerodynamic forces and moments are modeled by a Vortex-Lattice method. Based on those methods and the design parameter, a nonlinear flight dynamic model is build up in Simulink. This model is linearized and analyzed by numerical perturbation.

2.1 Equations of Motion

The origin of the equations of motion is Kane's dynamical equation,

$$\tilde{\mathbf{F}}_r + \tilde{\mathbf{F}}_r^{\star} = 0 \quad (r = 1, \ldots, p)\,, \tag{1}$$

where $\tilde{\mathbf{F}}_r$ are the generalized active forces, $\tilde{\mathbf{F}}_r^{\star}$ are the generalized inertial forces and p is the number of degrees of freedom of the system in the reference frame. In Eq. 1, the denotation

(a) Mechanical joint connection between two aircraft of the Experimental Multi-Body Aircraft

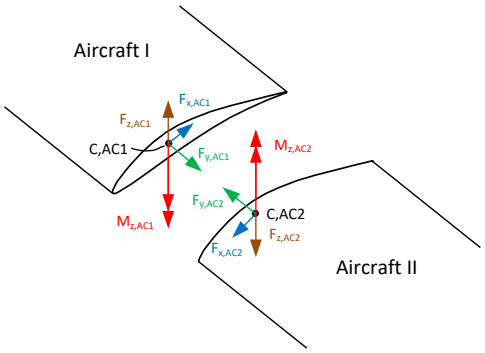

(b) Free body diagram of the joint connection

Figure 3: Mechanical joint connection for coupling two aircraft with pitch and roll degree of freedom

"generalized force" includes inertial and active forces as well as inertial and active moments (translation and rotation) [6]. Details are given in [8, 9]. The experimental Multi-Body aircraft consists of three coupled aircraft. Each individual aircraft has six degrees of freedom. Because of coupling, this number is reduced. Equivalent to the HAPS Multi-Body aircraft, the aircraft are coupled by a mechanical joint that allows a roll and pitch motion between the single aircraft. The used joint connection is illustrated in Figure 3(a). Every joint consists of two shafts: One shaft is fixed in one aircraft and the other shaft can be rotated around the pitch axis in the other aircraft. Both shafts are connected with a degree of freedom around the roll axis. The used joint prohibits a transfer of bending and torsional moment, but allows a yaw moment transfer as well as a transfer of all forces in all directions as illustrated in Figure 3(b). The selected connection results in non-holonomic constrains that are described by

$$\begin{aligned} \left({}^{N}\mathbf{v}^{C,AC1} - {}^{N}\mathbf{v}^{C,AC2}\right)\vec{e}_{\mathrm{xg}} &= 0 \qquad \left({}^{N}\mathbf{v}^{C,AC1} - {}^{N}\mathbf{v}^{C,AC2}\right)\vec{e}_{\mathrm{yg}} = 0 \\ \left({}^{N}\mathbf{v}^{C,AC2} - {}^{N}\mathbf{v}^{C,AC1}\right)\vec{e}_{\mathrm{zg}} &= 0 \qquad \left({}^{N}\omega^{A} - {}^{N}\omega^{B}\right)\vec{e}_{\mathrm{zg}} = 0 \end{aligned} \tag{2}$$

with $C, AC1$ as connection point at the first and $C, AC2$ at the second aircraft (cf. Figure 3(b)) and $\vec{e}_{\mathrm{xg}}$, $\vec{e}_{\mathrm{yg}}$ and $\vec{e}_{\mathrm{zg}}$ as unit vectors of the geodetic reference frame. In the case of the Experimental Multi-Body Aircraft with three aircraft, only the generalized speeds relating to the translational motion and yaw motion of one aircraft and the generalized speeds relating to the pitch and roll motion of every aircraft remain. Nevertheless, the number of generalized coordinates is higher than the number of generalized speeds. That results from the fact that the non-holonomic constrain equation relating to the yaw motion cannot be transferred into a holonomic constrain for the yaw angle. The kinematic differential equations allow a yaw angle between both aircraft if a roll and pitch rate occur simultaneously.

2.2 External Active Forces and Moments

The active forces and moments that have to be considered for the equations of motion are: aerodynamic forces (in the aerodynamic reference frame) $\mathbf{R}_A$, thrust (in the body fixed reference frame) $\mathbf{T}$ and weight (in the Newtonian frame) $\mathbf{W}$ of each aircraft as well as aerodynamic moments (in the aerodynamic reference frame) $\mathbf{M}_A$ and thrust moments (in the body fixed reference frame) $\mathbf{M}_T$. For each single aircraft, it is assumed that the thrust acts at the center of gravity. This results in a zero thrust moment. The active force at the jth aircraft in the body

fixed reference frame is then determined as

$$ {}^{b}\mathbf{F}_{A}^{CG,j} = \mathbf{T}_{b,a,j}\,\mathbf{R}_{A,a,j} + \mathbf{T}_{b,g,j}\,\mathbf{W}_{n,j} + \mathbf{T}_{b,j}, \tag{3} $$

where $\mathbf{T}_{b,a,j}$ is the transformation matrix from the aerodynamic reference frame (index a) to the body fixed reference frame (index b) and $\mathbf{T}_{b,n,j}$ is the transformation matrix from the geodetic reference frame index g to the body fixed reference frame for the jth aircraft. The active moment of the jth aircraft in the body fixed reference frame is computed with

$$ {}^{b}\mathbf{M}_{A}^{CG,j} = \mathbf{T}_{b,a,j}\,\mathbf{M}_{A,a,j} + \underbrace{\mathbf{M}_{b,F}}_{=0}. \tag{4} $$

The gravity of the jth aircraft is defined in the Newtonian reference frame as

$$ \mathbf{W}_{n,j} = [0, \quad 0, \quad m_j\,g]^T \tag{5} $$

where m_j is the mass of the jth aircraft and g is the gravitational acceleration. The thrust of the jth aircraft is calculated with

$$ \mathbf{T}_{b,j} = [F_j, \quad 0, \quad 0]^T \tag{6} $$

where F_j is the thrust of the jth engine.

Aerodynamic forces and moments are generated by the wing, horizontal stabilizer and vertical stabilizer. The overall wing is built up by the wings of the single aircraft. As a consequence, a wing with a high aspect ratio is formed. The aerodynamic forces and moments are calculated in MATLAB with the vortex lattice method described in [10]. For this purpose, the wing is divided into a finite number of surfaces. The flow conditions on every surface depend on both the air density and aerodynamic parameter (angle of attack, sideslip angle and airspeed) that are also a function of the yaw rate of the whole formation and the pitch and roll rate of every individual aircraft. The software tool Autolev / Motion Genesis computes those kinematic equations after the definition of motion constraints. Based on the aerodynamic conditions, the vortex lattice method determines lift, yaw (considering also the zero drag coefficient) and induced drag of every surface. By rotation of the normal vectors of the surfaces, flap deflections are considered. For the experimental Multi-Body aircraft every single aircraft is equipped with flaps along the complete left $\eta_{K,left}$ and right wing $\eta_{K,right}$ with 20 % flap chord. Based on the aerodynamic forces at every surface and the corresponding collocation point, lift, induced drag and yaw can be assembled to each single aircraft. If the surface collocation point of the complete wing belongs to the ith aircraft, the forces are assigned to the ith aircraft. The corresponding aerodynamic moments are calculated by the lever arm of the surface collocation point (that belongs to the ith aircraft) to the center of gravity of the ith aircraft. To consider the downwash, horizontal and vertical stabilizer are included to the vortex lattice computation. The forces and moments can be directly assigned to the corresponding aircraft. The influence of rudder ζ and elevator η with 30 % flap chord of vertical and 25 % flap chord of horizontal stabilizer is computed by rotation of the normal vector of the corresponding surfaces. Finally, the part of the zero drag is added to each aircraft.

As illustrated in Figure 3(a) there is a gap between two aircraft wings. This cap would lead to a flow from the down side to the upper side. For the experimental aicraft, straws are used for sealing between the two wings. This principle is equivalent to the connection of train wagons. In the aerodynamic model, however, the gap is neglected.

Table 2: Trim results of the experimental Multi-Body aircraft at an airspeed of 14 $\frac{\text{m}}{\text{s}}$ at sea level

	Aircraft 1	Aircraft 2	Aircraft 3
Angle of attack	$2.303°$	$2.303°$	$2.303°$
Thrust	3.976 N	3.505 N	3.976 N
Elevator deflection	$-14.994°$	$-3.759°$	$-14.994°$
Left wing flap	$5.107°$	$0°$	$2.879°$
Right wing flap	$2.879°$	$0°$	$5.107°$

2.3 Linear Analysis of the Experimental Multi-Body Aircraft

Based on the non-linear equations of motion, the flight dynamics of the experimental Multi-Body aircraft are trimmed. As flight conditions, an airspeed of 14 $\frac{\text{m}}{\text{s}}$ at sea level is assumed. The trim results are listed in Table 2. Afterwards, the aircraft was linearized at the trim point. The center aircraft is selected as main aircraft. This means that all generalized speeds and coordinates are taken into account while for the outer aircraft only the pitch and roll motion as well as the yaw angle is considered. Additionally to the previous introduced flight dynamic model, the difference of the yaw to the yaw angle of the main aircraft

$$\Delta\Psi_i = \Psi_2 - \Psi_i \quad \text{with} \quad i \in \{1, 3\} \tag{7}$$

is considered as state instead of the absolute yaw angle of every aircraft. The generalized coordinates relating to the navigation (three Cartesian coordinates and the yaw angle of formation) are neglected. The state vector

$$\mathbf{x} = \begin{bmatrix} q_{\text{AC2}}, \alpha_{\text{AC2}}, V_{\text{AC2}}, \gamma_{\text{AC2}}, r_{\text{AC2}}, \beta_{\text{AC2}}, \dots \\ p_{\text{AC2}}, \Phi_{\text{AC2}}, \mathbf{x}_{\text{AC1}}, \mathbf{x}_{\text{AC3}} \end{bmatrix}^T \quad \text{with} \quad \mathbf{x}_{\text{AC}i} = \begin{bmatrix} q_{\text{AC}i} \\ \Theta_{\text{AC}i} \\ p_{\text{AC}i} \\ \Phi_{\text{AC}i} \\ \Delta\Psi_{\text{AC}i} \end{bmatrix}^T \tag{8}$$

has 18 elements (resulting from generalized speeds and coordinates). A first analysis showed that the eigenvalues related to the yaw motion of every aircraft are close to the origin of the complex plane. Hence those two states are neglected and the state vector is reduced to 16 elements. The eigenvalues of the system are plotted in Figure 4. Four out of these eigenvalues are unstable. In total, the system has six real eigenvalues (two are unstable) and five complex conjugate eigenvalue pairs (one is unstable). Based on the eigenvectors, a clear separation between lateral, longitudinal and linkage eigenvalues is not possible. The eigenvectors show a strong coupling between all states in all modes. Nevertheless, a short period mode, a phygoid, a Dutch roll, an unstable spiral as well as roll and pitch linkage modes are recognizable.

3 CONTROL LAW DESIGN

Although the flight dynamics of a Multi-Body aircraft strongly deviate from classical aircraft, the cascade control principle for conventional aircraft was applied to the Multi-Body HAPS aircraft. To achieve flight path control, the following three loops were used: The basic flight control law shall ensure damping of rates, airspeed, and wing shape holding control, while the outer-loop is used for attitude control (flight control) and flight path control (flight guidance). The inner-loop was successfully designed with H_∞ loop shaping in the frequency domain.

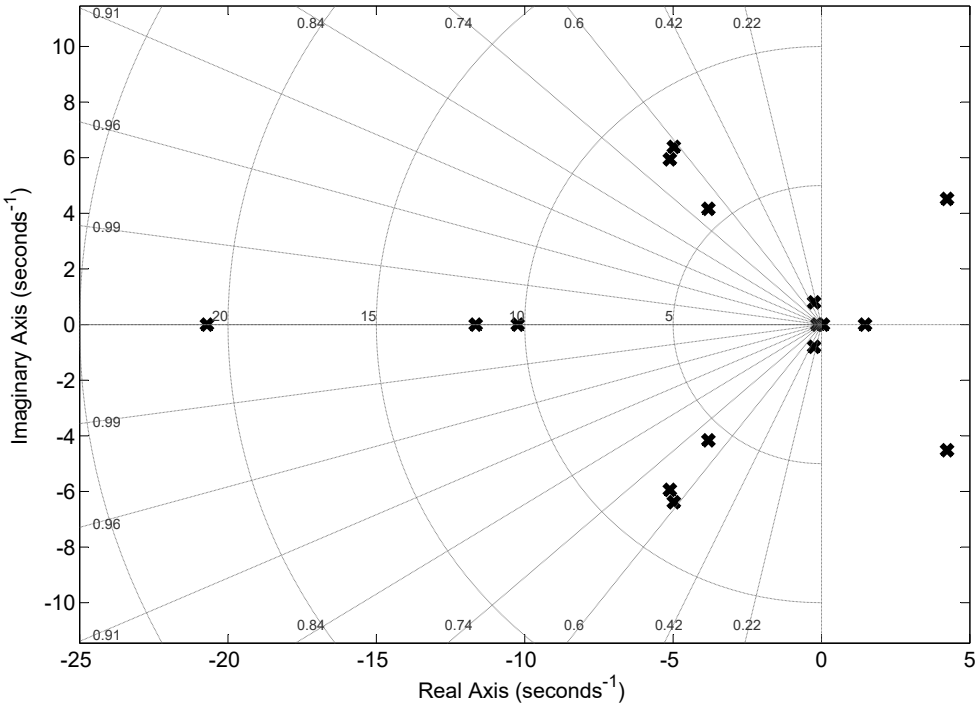

Figure 4: Illustration of the eigenvalues of the linearized experimental Multi-Body Aircraft in the complex plane

Nonlinear dynamic effects were summarized as uncertainties. The outer-loops were designed by classical root locus methods. With the design method, a robust inner-loop was designed that successfully stabilizes the plant and achieves wing shape holding, airspeed control as well as gust rejection. Especially the results of non-uniformly distributed gust load rejection underline the benefit of a Multi-Body HAPS aircraft in comparison to a one wing HAPS aircraft. In addition, azimuth tracking and altitude hold was successful verified in nonlinear simulations. [9]

In case of the experimental Multi-Body aircraft, the same flight control law structure and the same design method is applied but flight guidance is excluded. The pilot controls the aircraft via a remote controller and uses the pitch and roll angle as well as the airspeed as demand values for the flight control system. The used control law structure for the experimental Multi-Body aircraft is illustrated in Figure 5. In the following, the requirements and the design of inner-loop and flight control loop is explained in detail.

3.1 Requirements

The requirements for the flight control laws of the experimental Multi-Body aircraft are similar to the ones of the Multi-Body HAPS aircraft. The nominal plant has four unstable eigenvalues. The stabilization of the plant is the main requirement of the flight control law. After the Helios mishap, the NASA in its function as an investigation organization recommend the use of nonlinear methods in the aircraft modeling and the flight control law design [11]. Multi-Body aircrafts equations of motions are nonlinear due to the trigonometric functions caused by joint modeling and kinematic differential equations of the individual aircraft. The flight control law design process shall therefore consider those nonlinear effects. Due to gusts and turbulences,

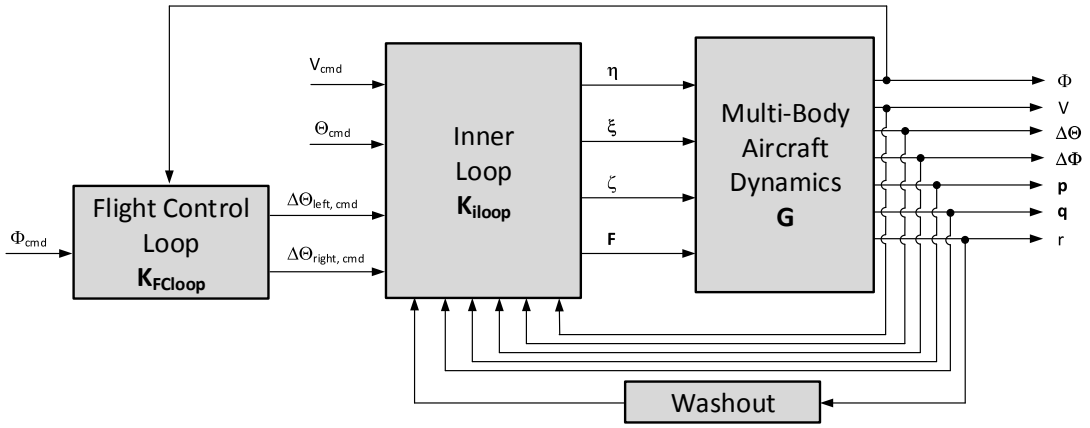

Figure 5: Block diagram for the cascade flight control law structure of the experimental Multi-Body aircraft

disturbances act on the aircraft and have to be rejected by damping of the rates [12] and by an airspeed controller. In case of the Multi-Body HAPS aircraft, a low energy consumption is a main requirement. This results in flying with a high lift coefficient close to the stall speed. To avoid stall, the flight control law has to achieve speed holding with high precision. Even though the experimental Multi-Body aircraft flies with an airspeed that is significant higher than the stall speed, airspeed holding shall be carried out fast and with high precision. Additional to the low airspeed, low energy consumption depends on wing shape. In a basic investigation it turned out that the deviations of the wing form has a negative impact on the induced drag. This leads to the requirement that the flight control law has to achieve wing shape holding. In case of the Multi-Body aircraft, wing shape holding means that the attitudes of every aircraft in the formation are equal. Deviations in wing shape are expressed by deviations in the pitch and bank angle that shall be controlled to zero. The bandwidth of the wing shape controller is defined with $\omega_B = 0.5\ \frac{\text{rad}}{\text{s}}$ with a maximum error of 10 %.

Regarding to airspeed and attitude control, additional requirements can be defined. The Multi-Body HAPS aircraft operates with 90 % of the maximum lift coefficient. Thus, a maximum drop of approximately 5 % of the airspeed in any flight condition is acceptable. A special risk of stall occurs in turns. The airspeed is increased on the outside of the curve and decrease on the inside of the curve. Due to the long span, the maximum drop of the airspeed on the inside of the curve aircraft has to be taken into account.

Quantitative requirements for the flight control law, like those described in MIL-F-9490D for piloted aircraft, do not exist for unmanned aircraft (especially not for HAPS). Based on the selected bandwidth for wing shape holding, attitude control shall be established with half bandwidth of wing shape holding because attitude control is within the outer-loop. Since airspeed control shall be established very fast, a bandwidth of $\omega_B = 2\ \frac{\text{rad}}{\text{s}}$ is selected for this loop.

3.2 Control Law Design

The control law design process for the experimental Multi-Body aircraft follows the same steps as the one for the Multi-Body HAPS aircraft to validate the methods. Details are described in [9]. In this section, only the most important facts are reviewed.

The inner-loop shall achieve stability, wing shape holding, damp pitch (each aircraft), roll (each

aircraft) as well as yaw rate (the latter one only rearding the formation) and controls the pitch angle as well as the airspeed. The differences in the wing shape are expressed by differences of pitch and roll angles of the outer aircraft relating to the second aircraft. For the attitude control, the differences in the pitch angle of the outer aircraft (left and right side pitch angle) have to follow a demand value. In straight flight, this demand value is zero, but if the aircraft turns, the demand value is defined by the flight control loop as will be explained later. In total, 13 output values (7 rates, 4 wing shape differences, pitch angle, and the airspeed) are controlled within the inner-loop. As input variables all elevator deflections are used. The left and right wing flap are summarized into a common aileron

$$\xi_{\text{AC}i} = \eta_{\text{K, right, AC}i} - \eta_{\text{K, left, AC}i} \quad \text{with} \quad i \in [1, 2, 3] \tag{9}$$

of every aircraft. The rudder is set to identical values for every aircraft. This leads to 13 input variables. The linearized state-space model used for the inner-loop design is

$$\begin{aligned} \dot{\mathbf{x}}(t) &= \mathbf{A}\mathbf{x}(t) + \mathbf{B}\mathbf{u}(t) \ , \\ \mathbf{y}(t) &= \mathbf{C}\mathbf{x} + \mathbf{D}\mathbf{u}(t) \end{aligned} \tag{10}$$

with $\mathbf{y}$ as control variables, $\mathbf{u}$ as control inputs and $\mathbf{x}$ as states. By applying the Laplace transformation (assuming that the feedforward matrix $\mathbf{D}$ is equal to zero), this state-space models yields the system

$$\begin{aligned} s\,\hat{\mathbf{x}}(s) &= \mathbf{A}\hat{\mathbf{x}}(s) + \mathbf{B}\hat{\mathbf{u}}(s) \ , \\ \hat{\mathbf{y}}(s) &= \mathbf{C}\hat{\mathbf{x}}(s) \end{aligned} \tag{11}$$

that describes the plant in the frequency domain. Hence, the transfer function of the plant for inner-loop design is determined by

$$\mathbf{G}(s) = \hat{\mathbf{y}}(s)\ \hat{\mathbf{u}}^{-1}(s) = \mathbf{C}\left[s\,\mathbf{I} - \mathbf{A}\right]^{-1}\mathbf{B}. \tag{12}$$

Those transfer functions have to be normalized to maximum input and output values by

$$\mathbf{G}_n = \mathbf{D}_e^{-1}\,\mathbf{G}\,\mathbf{D}_u\,. \tag{13}$$

before applying the H_∞ control law synthesis. The matrix $\mathbf{D}_e$ represents the maximum acceptable output values while the matrix $\mathbf{D}_u$ defines the maximum acceptable input values. All rates shall not exceed maximum values of 5°. The maximum wing shape differences are defined by 1°. The airspeed shall remain a constant value and a maximum drop of $0.5\ \frac{\text{m}}{\text{s}}$ is acceptable. The pitch angle variation relating to trimmed condition shall be within the interval of $\pm 5^\circ$. All aerodynamic surfaces shall not exceed values of $\pm 10^\circ$ relating to the trim values. A maximum increase for every engine of 10 N is acceptable. The performance weight for wing shape differences, pitch angles and airspeed are defined by the requirements. Control input with a frequency above 5 Hz shall be avoided. This is defined by weighting the control values depending on the frequency. The uncertainty is described as unstructured uncertainty in the additive perturbation configuration. The uncertain parameters are calculated by differences in the phase space (every deviation of the state variable as a function of every input and state variable) between the linear trajectory and the fully nonlinear trajectory [9]. By applying the H_∞ to the augmented plant that includes the linear model of the system as well as the performance and control activity weight and uncertainty description, a controller of order 38 is derived. By using the balanced truncation, the order of the control law for the inner-loop is reduced to 18. The control law is robust stable against the modelled uncertainties.

For turned flight, a washout filter of the yaw is integrated in the control loop. This destabilizes the closed loop of nominal plant and inner-loop. A stabilization is achieved by a bank angle controller. This change is expected since the spiral mode has to be unstable for turned flight. The bank angle control law bases on the principle that there is a lift imbalance between left and right side of the formation. The differences in the lift are established by different pitch angles of the two outer aircraft. Those values $\Delta\Theta_{\text{left, cmd}}$ and $\Delta\Theta_{\text{right, cmd}}$ represent the demand values for the wing shape controller. Because the bank angle controller assigns adverse signals (a positive and a negative one) of similar magnitude ξ_{bank} as demand values, i.e.

$$\begin{aligned} \Delta\Theta_{\text{left, cmd}} &= +\xi_{\text{bank}} \\ \Delta\Theta_{\text{right, cmd}} &= -\xi_{\text{bank}} \end{aligned}, \tag{14}$$

a roll moment occurs. The bank angle controller is designed with the root locus method [12]. The transfer function from ξ_{bank} to the bank angle is used. Therefore, the system is reduced by the balanced truncation to a second order system. The corresponding control law is

$$\xi_{\text{bank}} = k_{\xi\Phi}\left(\Phi_{\text{cmd}} - \Phi_{\text{AC2}}\right) \tag{15}$$

and the proportional gain is determined with $k_{\xi\Phi} = 2.1$. With this approach, bank angle is controlled for the experimental Multi-Body aircraft and the closed loop is stabilized.

3.3 Nonlinear Simulation Results

The results of the nonlinear closed-loop simulations for a change in the commanded pitch and bank angle of the experimental Multi-Body aircraft are illustrated in Figures 6 and 7. In case of a pitch angle command input, all pitch angles respond simultaneously. This indicates that the wing shape controller relating to the pitch angle works well. A steady error occurs in the pitch angle. This was not the case in linear simulations. The corresponding elevator deflections are low. No high frequency deflections are identified. Deviations in the bank angle are very low and, hence, the requirements of the wing shape holding relating to the bank angle is completely fulfilled. The drop in the airspeed is very low and hence the requirements of airspeed control are also fulfilled. The results are comparable with the nonlinear simulation studies of the Multi-Body HAPS aircraft [9].

In case of a change of the commanded bank angle, the initial reaction of the formation is very fast. But afterwards it takes a long time until a steady value of the bank is achieved. This is not comparable to the results of Multi-Body HAPS aircraft. The functionality of the attitude control loop is obviously in the pitch angles of the individual aircraft. Also in lateral motion control surface deflections are within limits and the drop of the airspeed is very low. In summary, the designed control law seems to be feasible for usage in a flight test under real world conditions.

4 IMPLEMENTATION OF THE FLIGHT CONTROL LAW TO THE EXPERIMENTAL MULTI-BODY AIRCRAFT

The developed flight control law has to be implemented for use in the experimental demonstrator. Therefore, a flight control is required that measures the control variables, computes the flight control law and sets the actuators.

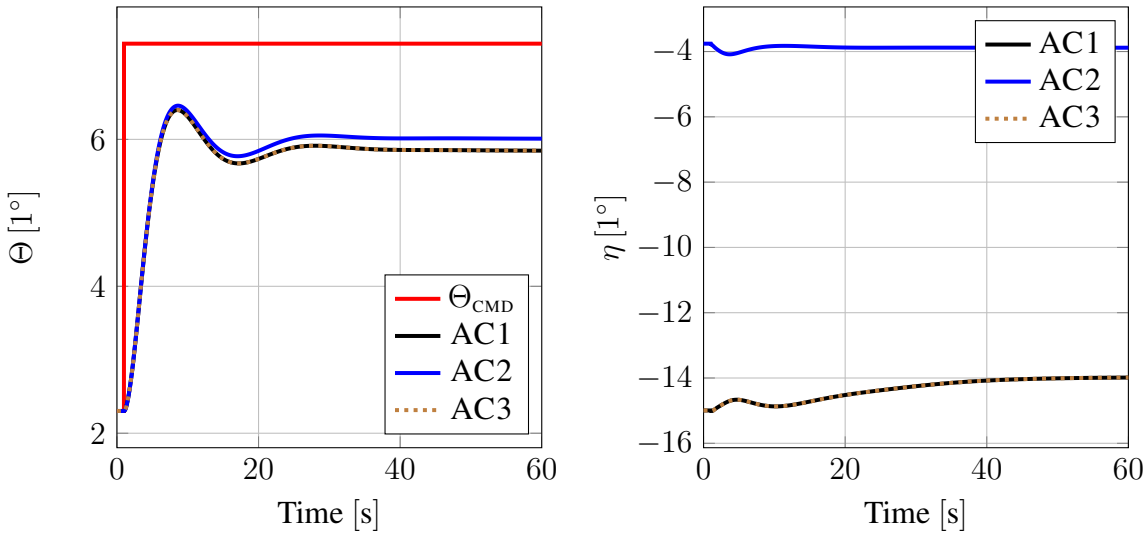

(a) Pitch angles

(b) Elevators

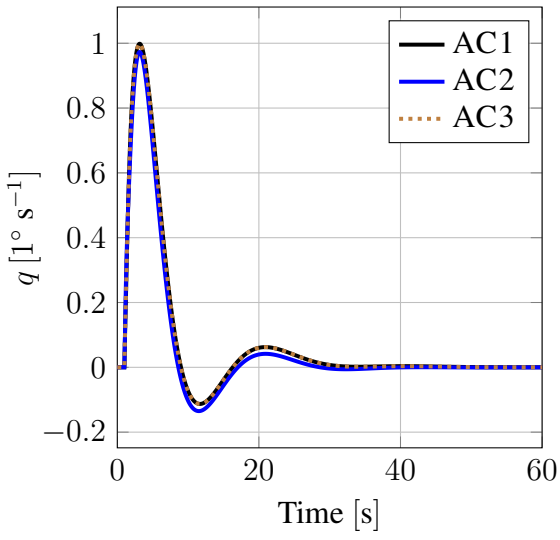

(c) Pitch rate

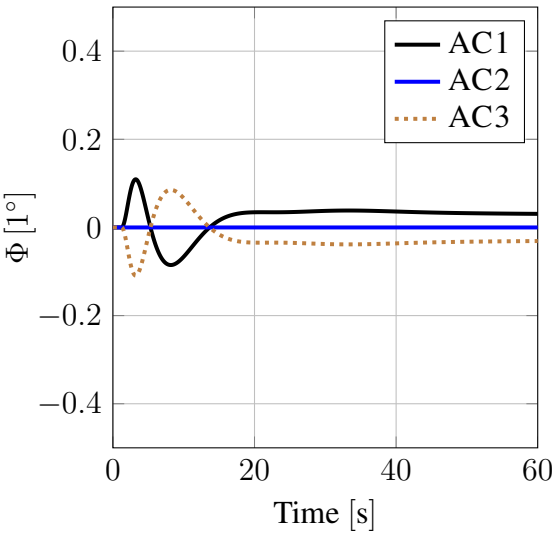

(d) Bank angles

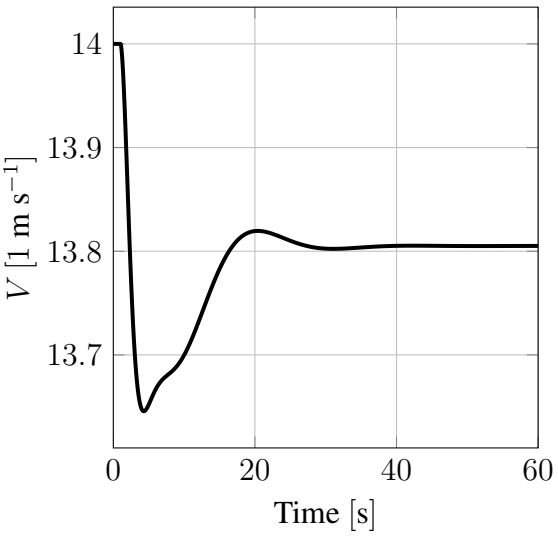

(e) Airspeed

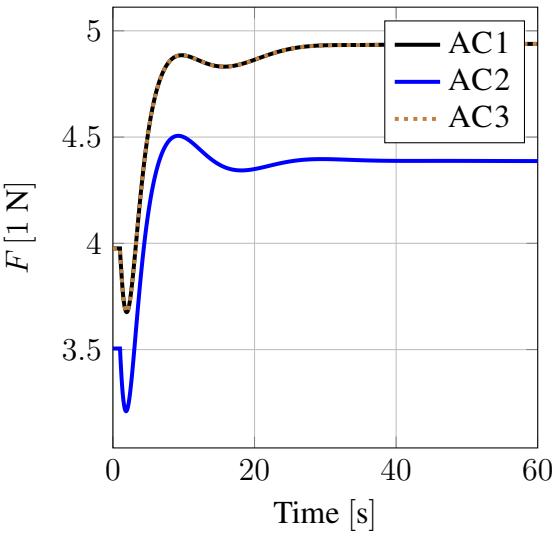

(f) Engine thrust

Figure 6: Nonlinear simulation results of inner-loop for a step input to increase the pitch angle command by 5°

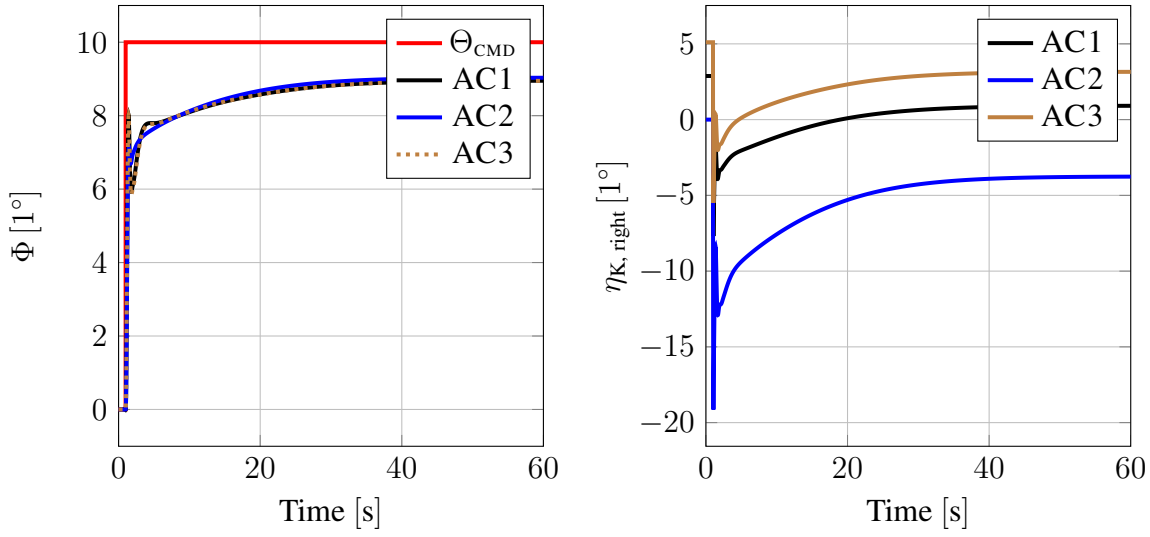

(a) Bank angles

(b) Right wing flaps

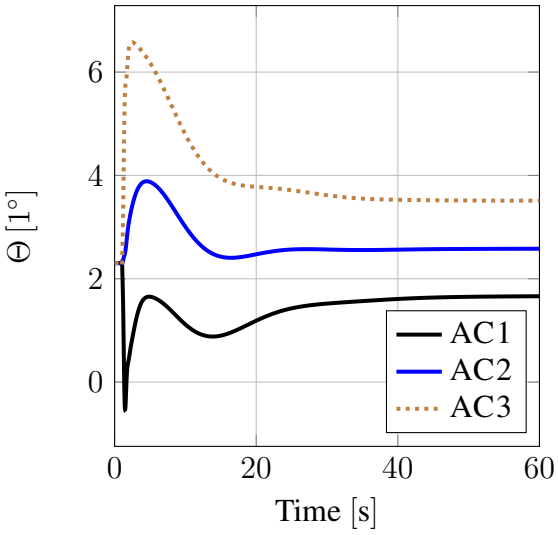

(c) Pitch angles

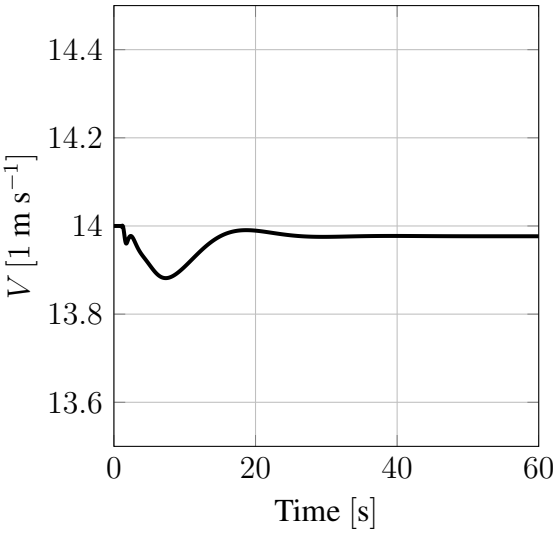

(d) Airspeed

Figure 7: Nonlinear simulation results of inner-loop for a step input to bank angle command of 10°

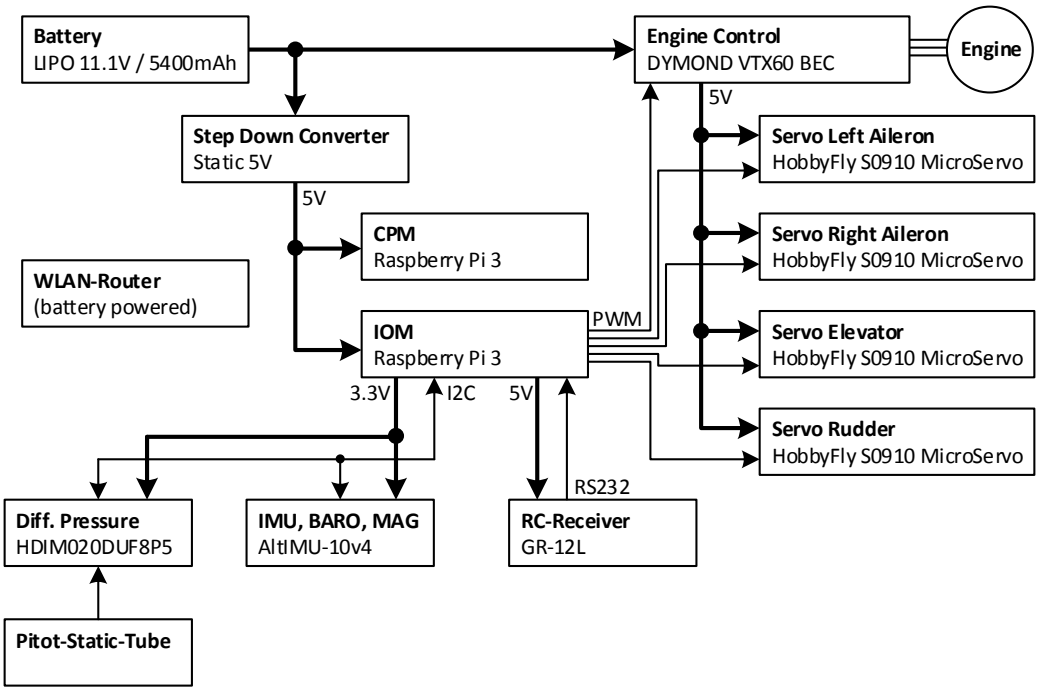

Figure 8: Flight Control System architecture of the central aircraft

4.1 Flight Control System Architecture

Every aircraft of the experimental Multi-Body aircraft is equipped with an Input/Output Module (IOM) that reads sensor data and sets the controls. Additionally, the second (central) aircraft has a Core Processing Module (CPM) on which the flight control laws are processed. The system architecture for the second aircraft is illustrated in Figure 8. The IOM gets signals from the IMU (inertial measurement unit), BARO (static pressure) and MAG (magnetic field), combined by a *Pololu AltIMU-10 v4* sensor, and from the *FirstSensor HDIM020DUF8P5* differential pressure sensor by an I2C (Inter-Integrated Circuit) data bus. The remote control receiver sends the received pilot inputs by an RS232 (serial communication) bus to the IOM. In contrast to the central aircraft, the two outer aircraft of the formation have no CPM and the IOM reads only the sensors IMU , BARO and MAG. The IOM sensor values of the two outer aircraft have to be transmitted to the CPM of the middle aircraft. State of the art solutions in aircraft systems use a wired bus connection. This is not applicable for the experimental Multi-Body aircraft since a wired connection would influence the connection of two coupled aircraft. Hence, a wireless data transfer is used for remote sensing. There are different types of wireless communication like radio transmitters, analog and digital cellular networks, infrared, Bluetooth or wireless local area networks (WLAN) [13]. In case of the Multi-Body Aircraft, the WLAN solution is considered, because it can be operated as a mobile infrastructure (with mobile access point hubs) with a wide range and a stream data rate of more than 500 megabyte per second in IEEE standard 802.11ac [14, 15]. The flight control system is build using commercial-off-the-shelf hardware. The computers for the IOMs and CPM are *Raspberry PI 3* single-board computer. Each computer is equipped by a wireless adapter working with 2.4 GHz. Because the remote controller transmits data in the same frequency band, an external *AUKEY WF-R3* WLAN stick for the 5 GHz band is used. The *TP-Link M7350* hub works as a wireless access point that deals with the wireless standards IEEE 802.11a, IEEE 802.11b, IEEE 802.11g, and IEEE 802.11n. After computing the actuator signals by the flight control laws, the CPM transmits

the commands to the IOM. Every IOM is connected with four servo motors for left and right side aileron, elevator and rudder as well as to an engine controller by pulse-width modulation (PWM) signals. The power for the computer as well as actuators and sensors is supplied by an 11.1 V battery. Based on the power supply and the system architecture, the flight control system of the experimental Multi-Body aircraft is designed as simplex. Accordingly, the risk that a single failure causes loss of the aircraft cannot completely be ruled out. This is acceptable, since the experimental aircraft is used as a technology demonstrator.

4.2 Software Implementation

The *Raspbian* Linux operation system runs on the CPM and IOM computer. The software is written in *C++*. The software of the flight control system has to fulfill real-time-requirements. Although the final design has to meet hard real-time requirements, the current experimental system fulfills soft real-time requirements only in order to reduce the development effort. CPM and IOMs run independently and asynchronous. Regarding the Open Systems Interconnection Model (OSI) that is a conceptual model that characterizes and standardizes the communication functions, the data transfer between IOM and CPM is established. The wireless connection compensates for the physical layer and the IEEE 802.11 standard is used for the data link layer. For the network layer, the Internet Protocol is used. The fourth layer of the OSI model represents the transport layer. In case of the flight control system for the experimental Multi-Body aircraft, the User Datagram Protocol (UDP) services are implemented. This follows from the fact that a packet delay is more critical than a packet loss in a flight control system. To guarantee a certain quality of service in the data transmission, a Data Distribution Service (DDS) is used between the transport layer and the application layer. This DDS works with the so-called publish-subscribe principle. Every IOM publishes the sensor values to an imaginary data space and the CPM subscribe those values. Since DDS implementation requires a high effort and network knowledge, the Robot Operating System (ROS) 2 is used to establish the DDS. ROS 2 fits the requirements relating to distributed systems like in the case of the experimental Multi-Body Aircraft. ROS 2 is directly integrated in the source code of the IOM and CPM. [16–18]

The software running on the IOM is structured as follows. On the input side, the IOM communicates on separate threads with the several sensors and puts the received data into a ring buffer. A publisher thread publishes the newest data of the buffer to the network on a constant frequency of 100 Hz. On the output side, the IOM subscribes the command messages of the CPM and stores the data into a ring buffer. To ensure that the control surfaces changes their values synchrony, the CPM sends a set command to the IOM. After having received this set signal, the buffer pointer is updated which leads to an immediate update of the actuator command output.

Onside the CPM, one subscriber thread for each IOM collects the published sensor data and puts them into a ring buffer. Inside, a time controlled loop one thread for each aircraft first copies data from the ring buffer to a data structure. This loop runs with a constant frequency of 100 Hz. The flight control laws are a separate *C++* function that is generated by the *Embedded Coder* of MATLAB. This ensures that the tested controller of the nonlinear *Simulink* simulation is directly integrated in the source code of the CPM. The data structure with the sensor data is hand over to the flight control law function and as an output a data structure is generated that includes the command values for the actuators. These commands are published to the IOM and at the end of the time controlled loop, the set signal is published to the IOM.

In [19] the time delay of the flight control system is investigated. In a ground based test cam-

Figure 9: Take-off construction of the experimental Multi-Body aircraft installed on the top of a car

paign, it turned out that a time delay of 20 ms can be expected. This value is slightly higher in comparison to a wired Ethernet connection.

5 FLIGHT TEST CAMPING

The flight test preparation has been completed. Due to technical and regulatory issues, the flight test had not been carried out on time to be included in the present paper. While the procedure of the flight test, nevertheless, is described in detail, actual results will be presente in an upcoming oral presentation.

In contrast to the Multi-Body HAPS Aircraft, the experimental Multi-Body Aircraft is not linked in its mission altitude, but was already connected on the ground. After several tests, the decision was made that the formation shall be equipped with a landing gear and, hence, a self-take-off is not possible. Like the Facebook Aquila, the aircraft shall be accelerated to the lift-off speed by a car. Therefore a construction made by wood is installed on the top of a car. The bearings between the aircraft are already connected and each aircraft is fixed by a clutch on the construction. A movement of the individual aircraft is not possible until the clutches are released. Before take-off, the pitch angle of all aircraft is set to the trimmed condition as listed in Table 2. Afterwards, the trim values for thrust and aerodynamic surfaces are set and the car accelerates with the aircraft on top to the lift-off speed. If a steady velocity is achieved, the clutches for every aircraft are released synchronously by pulling a cable that connects all clutches. If the aircraft lift off from the construction, the car stops in order to avoid a collision. The car equipped with the experimental take-off construction is illustrated in Figure 9.

6 SUMMARY AND OUTLOOK

In previous numerical investigation, the concept of a Multi-Body aircraft was successfully evaluated for application as High Altitude Pseudo Satellite Technology. The aircraft was designed, a flight mechanical model was build and the control laws for the unstable plant were designed. The practical proof of controlling such an aircraft formation is the necessary next step. The goal

of this paper was to describe the validation process to show that a practical operation of a Multi-Body Aircraft with the selected control law structure is possible. Therefore, the same principles of modeling the flight dynamics and designing the control laws for the Multi-Body HAPS aircraft were applied to a small scaled experimental Multi-Body aircraft. A control law that is able to stabilize the aircraft and achieve attitude and airspeed control was designed and verified in nonlinear simulations. The hard- and software integration of the flight control law to a flight control system that communicates using WLAN between the single aircraft was described and successfully tested. The operation of the demonstrator requires an adequate take-off procedure. Therefore a car with a take-off construction was used that accelerates the experimental Multi-Body aircraft up to the lift-off speed. A common release of the clutches ensures a synchronous lift-off of all aircraft.

The actual flight test results are pending, mainly due to regulatory issues. As the flight test shall be carried out soon after the publication, their results will be shown in a corresponding oral presentation of the paper. As an upcoming, further step two more aircraft will be connected to the formation after the successful flight tests with three aircraft. Consequently, the resulting formation of five connected aircraft will be tested in flight, to reaffirm the practical applicability of the unmanned Multi-Body aircraft technology.

7 References

[1] Lee, B., Park, P., and Kim, C. (2015). *Power Managements of a Hybrid Electric Propulsion System Powered by Solar Cells, Fuel Cells, and Batteries for UAVs*. Springer.

[2] Kovach, S. (2017). *Google's parent company killed its solar-powered internet-drone program*.

[3] Levin, A. (2016). *Accident Involving Facebook Experimental Drone Under Investigation*. Bloomberg Technology.

[4] DARPA (2007). *Vulture Program*. Broad Agency Announcement (BAA) Solicitation 07-51.

[5] Lockett, B. (2013). *Flying Aircraft Carriers of the Usaf: Wing Tip Coupling*. Lockett-Books.

[6] Kane, T. R. and Levinson, D. A. (1985). *Dynamics, Theory and Applications*. McGraw Hill.

[7] Levinson, D. A. and Kane, T. R. (1990). *AUTOLEV - A new Approach to Multibody Dynamics*. Springer.

[8] Köthe, A. and Luckner, R. (2015). *Flight Mechanical Modeling and Analysis of Multi-Body Aircraft*. International Forum on Aeroelasticity and Structural Dynamics (IFASD), St. Petersburg, Russia.

[9] Köthe, A. and Luckner, R. (2017). *Flight Path Control for a Multi-Body HALE Aircraft*. 4th CEAS Specialist Conference on Guidance, Navigation & Control.

[10] Katz, J. and Plotkin, A. (2001). *Low-Speed Aerodynamics*. Cambridge Aerospace Series. Cambridge University Press.

[11] Noll, T. E., Brown, J. M., Perez-Davis, M. E., et al. (2004). *Investigation of the Helios prototype aircraft mishap volume I mishap report*. National Aeronautics and Space Administration.

[12] Brockhaus, R., Alles, W., and Luckner, R. (2013). *Flugregelung*. Springer-Verlag.

[13] Tse, D. and Viswanath, P. (2005). *Fundamentals of wireless communication*. Cambridge university press.

[14] Ilyas, M. and Ahson, S. A. (2005). *Handbook of wireless local area networks: Applications, Technology, Security, and Standards*. CRC Press.

[15] Bejarano, O., Knightly, E. W., and Park, M. (2013). *IEEE 802.11 AC: From Channelization to Multi-User MIMO*, vol. 51. IEEE Communications Magazine.

[16] Furrer, F., Burri, M., Achtelik, M., et al. (2016). *Robot Operating System (ROS): The Complete Reference (Volume 1)*. Springer International Publishing.

[17] Bellavista, P., Corradi, A., Foschini, L., et al. (2013). *Data Distribution Service (DDS): A performance comparison of OpenSplice and RTI implementations*. IEEE.

[18] Hartanto, R. and Eich, M. (2014). Reliable, cloud-based communication for multi-robot systems. IEEE, Technologies for Practical Robot Applications (TePRA), 2014 IEEE International Conference.

[19] Köthe, A., Behrens, A., Nowka, D., et al. (2017). *Transport Delay in the Distributed Flight Control System of an Experimental Multi-Body Aircraft with Wireless Communication*. 4th CEAS Specialist Conference on Guidance, Navigation & Control.

COPYRIGHT STATEMENT